FILTERS, COLOR CORRECTION AND CALIBRATION UNCERTAINTIES OF COMMON INSTRUMENTS

Frédéric Galliano

Université Paris-Saclay, Université Paris Cité, CEA, CNRS, AIM, 91191, Gif-sur-Yvette, France

October 14, 2022

Contents

1 GENERAL FORMULAE FOR SYNTHETIC PHOTOMETRY **4**
1.1 Photomultipliers . . . 4
1.2 Bolometers . . . 4
1.3 The Synthetic Photometry Subroutine . . . 4

2 2MASS **4**
2.1 Filters and Color Correction . . . 5
2.2 Calibration errors . . . 5

3 Akari FIS **5**
3.1 Filters and Color Correction . . . 5
3.2 Calibration errors . . . 7

4 Akari IRC **7**
4.1 Filters and Color Correction . . . 7
4.2 Calibration errors . . . 8

5 IRAS **8**
5.1 Filters and Color Correction . . . 8
5.2 Calibration errors . . . 8

6 Herschel PACS **9**
6.1 Filters and Color Correction . . . 9
6.2 Calibration errors . . . 9

7 Herschel SPIRE **9**
7.1 Filters and Color Correction . . . 10
7.2 Calibration errors . . . 10

8 MSX Galactic Plane Survey **11**
8.1 Filters and Color Correction . . . 11
8.2 Calibration errors . . . 11

9 Planck HFI **11**
9.1 Filters and Color Correction . . . 12
9.2 Calibration errors . . . 12

10 Spitzer IRAC **12**
10.1 Filters and Color Correction . . . 13
10.2 Calibration errors . . . 13

11 Spitzer MIPS **13**
11.1 Filters and Color Correction . . . 14
11.2 Calibration errors . . . 14

12 WISE **14**

12.1 Filters and Color Correction 15
12.2 Calibration errors 15

13 DIRBE **16**
13.1 Filters and Color Correction 16
13.2 Calibration errors 16

14 NIKA2 **17**
14.1 Filters and Color Correction 17
14.2 Calibration errors 17

References **17**

Filter label	Band Center		Spectral Width		Wavelength Bounds	
2MASS1	1.24 μm	2.43×10^5 GHz	0.213 μm	4.25×10^4 GHz	1.12 μm	1.34 μm
DIRBE1	1.25 μm	2.40×10^5 GHz	0.297 μm	5.53×10^4 GHz	1.13 μm	1.43 μm
2MASS2	1.66 μm	1.80×10^5 GHz	0.247 μm	2.73×10^4 GHz	1.53 μm	1.77 μm
2MASS3	2.16 μm	1.39×10^5 GHz	0.274 μm	1.77×10^4 GHz	2.02 μm	2.29 μm
DIRBE2	2.20 μm	1.36×10^5 GHz	0.35 μm	2.10×10^4 GHz	2.06 μm	2.40 μm
AKARI_IRC1	2.40 μm	1.25×10^5 GHz	0.91 μm	5.06×10^4 GHz	1.91 μm	2.82 μm
AKARI_IRC2	3.2 μm	9.37×10^4 GHz	1.09 μm	3.18×10^4 GHz	2.71 μm	3.8 μm
WISE1	3.4 μm	8.94×10^4 GHz	0.86 μm	2.38×10^4 GHz	2.89 μm	3.8 μm
DIRBE3	3.5 μm	8.56×10^4 GHz	0.88 μm	2.13×10^4 GHz	3.11 μm	4.0 μm
IRAC1	3.5 μm	8.46×10^4 GHz	0.67 μm	1.61×10^4 GHz	3.2 μm	3.9 μm
AKARI_IRC3	4.1 μm	7.31×10^4 GHz	1.65 μm	2.54×10^4 GHz	3.7 μm	5.3 μm
IRAC2	4.5 μm	6.68×10^4 GHz	0.91 μm	1.36×10^4 GHz	4.0 μm	5.0 μm
WISE2	4.6 μm	6.51×10^4 GHz	1.01 μm	1.43×10^4 GHz	4.1 μm	5.1 μm
DIRBE4	4.9 μm	6.12×10^4 GHz	0.65 μm	8100 GHz	4.6 μm	5.2 μm
IRAC3	5.7 μm	5.25×10^4 GHz	1.26 μm	1.17×10^4 GHz	5.1 μm	6.3 μm
AKARI_IRC4	7.0 μm	4.28×10^4 GHz	2.44 μm	1.49×10^4 GHz	5.9 μm	8.3 μm
IRAC4	7.8 μm	3.82×10^4 GHz	2.59 μm	1.28×10^4 GHz	6.6 μm	9.2 μm
MSX1	8.3 μm	3.62×10^4 GHz	4.2 μm	1.81×10^4 GHz	6.5 μm	10.6 μm
AKARI_IRC5	9.0 μm	3.33×10^4 GHz	4.7 μm	1.86×10^4 GHz	6.7 μm	11.4 μm
AKARI_IRC6	11.0 μm	2.72×10^4 GHz	5.1 μm	1.25×10^4 GHz	8.8 μm	13.9 μm
WISE3	11.6 μm	2.59×10^4 GHz	7.8 μm	1.78×10^4 GHz	8.2 μm	16.0 μm
IRAS1	12.0 μm	2.50×10^4 GHz	6.5 μm	1.68×10^4 GHz	8.0 μm	14.5 μm
DIRBE5	12.0 μm	2.50×10^4 GHz	7.6 μm	1.58×10^4 GHz	8.8 μm	16.4 μm
MSX2	12.1 μm	2.47×10^4 GHz	1.91 μm	3900 GHz	11.2 μm	13.1 μm
MSX3	14.7 μm	2.05×10^4 GHz	2.23 μm	3110 GHz	13.6 μm	15.8 μm
AKARI_IRC7	15.0 μm	2.00×10^4 GHz	6.1 μm	7300 GHz	13.1 μm	19.2 μm
AKARI_IRC8	18.0 μm	1.66×10^4 GHz	10.8 μm	8700 GHz	14.6 μm	25.4 μm
MSX4	21.3 μm	1.40×10^4 GHz	6.7 μm	4200 GHz	18.6 μm	25.3 μm
WISE4	22.1 μm	1.36×10^4 GHz	5.4 μm	2990 GHz	20.7 μm	26.1 μm
MIPS1	23.7 μm	1.27×10^4 GHz	6.4 μm	3400 GHz	21.0 μm	27.4 μm
AKARI_IRC9	24.0 μm	1.25×10^4 GHz	6.2 μm	3400 GHz	20.6 μm	26.8 μm
IRAS2	25.0 μm	1.20×10^4 GHz	11.5 μm	6800 GHz	17.5 μm	29.0 μm
DIRBE6	25.0 μm	1.20×10^4 GHz	8.6 μm	6000 GHz	16.9 μm	25.6 μm
IRAS3	60 μm	5000 GHz	36 μm	3300 GHz	42 μm	78 μm
DIRBE7	60 μm	5000 GHz	28.9 μm	2790 GHz	43 μm	72 μm
AKARI_FIS1	65 μm	4600 GHz	23.7 μm	1700 GHz	54 μm	78 μm
PACS1	70 μm	4300 GHz	23.6 μm	1390 GHz	61 μm	84 μm
MIPS2	71 μm	4200 GHz	30.5 μm	1710 GHz	59 μm	90 μm
AKARI_FIS2	90 μm	3300 GHz	45 μm	2000 GHz	63 μm	108 μm
IRAS4	100 μm	3000 GHz	40 μm	1250 GHz	80 μm	120 μm
DIRBE8	100 μm	3000 GHz	39 μm	1310 GHz	77 μm	117 μm
PACS2	100 μm	3000 GHz	36 μm	1030 GHz	86 μm	121 μm
AKARI_FIS3	140 μm	2140 GHz	63 μm	850 GHz	121 μm	183 μm
DIRBE9	140 μm	2140 GHz	74 μm	1000 GHz	117 μm	190 μm
MIPS3	156 μm	1920 GHz	41 μm	510 GHz	136 μm	177 μm
AKARI_FIS4	160 μm	1870 GHz	41 μm	450 GHz	145 μm	187 μm
PACS3	160 μm	1870 GHz	76 μm	840 GHz	131 μm	207 μm
DIRBE10	240 μm	1250 GHz	134 μm	640 GHz	192 μm	330 μm
SPIRE1	250 μm	1200 GHz	73 μm	350 GHz	214 μm	287 μm
HFI1	350 μm	860 GHz	114 μm	264 GHz	307 μm	420 μm
SPIRE2	350 μm	860 GHz	101 μm	249 GHz	301 μm	400 μm
SPIRE3	500 μm	600 GHz	185 μm	220 GHz	420 μm	600 μm
HFI2	550 μm	550 GHz	171 μm	167 GHz	470 μm	650 μm
HFI3	850 μm	350 GHz	234 μm	98 GHz	740 μm	970 μm
HFI4	1380 μm	217 GHz	410 μm	64 GHz	1200 μm	1600 μm
HFI5	2100 μm	143 GHz	660 μm	43 GHz	1820 μm	2480 μm
HFI6	3000 μm	100 GHz	900 μm	29.7 GHz	2590 μm	3500 μm

1 GENERAL FORMULAE FOR SYNTHETIC PHOTOMETRY

1.1 Photomultipliers

A photomultiplier (like IRAC, MIPS, ISOCAM, etc.), counts the number of photons received by the detector, whatever their energy is. The spectral shape of the SED is important to derive the proper integrated flux within the band, in order to perform reliable color correction or synthetic photometry.

The number of photons per unit time, per surface area and per bin of frequency, from an incident flux F_ν is:

$$\frac{\mathrm{d}N_\gamma}{\mathrm{d}t\,\mathrm{d}A\,\mathrm{d}\nu} = \frac{F_\nu}{h\nu}. \tag{1}$$

If we note $R(\nu)$, the quantum efficiency of the filter in electrons per photons, then the rate of electrons per unit surface is:

$$\frac{\mathrm{d}N_e}{\mathrm{d}t\,\mathrm{d}A} = \int \frac{F_\nu}{h\nu} R(\nu)\,\mathrm{d}\nu. \tag{2}$$

Each instrument has a specific flux convention $F_\nu^{\mathrm{conv.}}$, such that the flux in the band $F_{\nu_0}^{\mathrm{band}}$ is the interpolated value of this specific SED at the nominal wavelength of the bandpass: $F_{\nu_0}^{\mathrm{band}} = F_\nu^{\mathrm{conv.}}(\nu_0)$. For a general SED, and any flux convention, the quoted flux in the band will be:

$$F_{\nu_0}^{\mathrm{band}} = F_\nu^{\mathrm{conv.}}(\nu_0) \times \frac{\mathrm{d}N_e^{\mathrm{actual}}}{\mathrm{d}N_e^{\mathrm{conv.}}} \tag{3}$$

$$= \frac{\displaystyle\int F_\nu R(\nu) \left(\frac{\nu_0}{\nu}\right) \mathrm{d}\nu}{\displaystyle\int \left(\frac{F_\nu^{\mathrm{conv.}}(\nu)}{F_\nu^{\mathrm{conv.}}(\nu_0)}\right) R(\nu) \left(\frac{\nu_0}{\nu}\right) \mathrm{d}\nu}. \tag{4}$$

If the convention is the common $F_\nu^{\mathrm{conv.}} \propto \nu^{-\alpha}$, then the photometry is:

$$F_{\nu_0}^{\mathrm{band}} = \frac{\displaystyle\int F_\nu R(\nu) \left(\frac{\nu_0}{\nu}\right) \mathrm{d}\nu}{\displaystyle\int R(\nu) \left(\frac{\nu_0}{\nu}\right)^{\alpha+1} \mathrm{d}\nu}. \tag{5}$$

1.2 Bolometers

A bolometer integrates the power received whatever the photon number count is. The power received per unit area, per unit frequency, is:

$$\frac{\mathrm{d}E}{\mathrm{d}t\,\mathrm{d}A\,\mathrm{d}\nu} = F_\nu. \tag{6}$$

If we note $R(\nu)$ the spectral response of the filter, the quoted flux in the band is then:

$$F_{\nu_0}^{\mathrm{band}} = \frac{\displaystyle\int F_\nu R(\nu)\,\mathrm{d}\nu}{\displaystyle\int \left(\frac{F_\nu^{\mathrm{conv.}}(\nu)}{F_\nu^{\mathrm{conv.}}(\nu_0)}\right) R(\nu)\,\mathrm{d}\nu}. \tag{7}$$

1.3 The Synthetic Photometry Subroutine

The subroutine `synthetic_photometry` in the module `instrument_filters` performs synthetic photometry for all the filters listed in these notes. It builds an adaptative grid in wavelength in order to enforce a 10^{-3} accuracy on the derived quoted flux.

The accuracy of the comparison of the results of this subroutine to color correction tables given in observers' manuals is often more sensitive to the accuracy of the interpolation of the model (especially for very steep spectra), rather than to the actual accuracy of the integration. In any case, the systematic comparison shows that our routine is consistent with this table, most of the time, better than $1\,\%$.

2 2MASS

2.1 Filters and Color Correction

According to the 2MASS explanatory supplement, the filters provided are $\lambda R(\lambda)$, and are designed to be directly integrated over F_λ. Changing the SED to frequency dependence, we get:

$$F_{\nu_0}^{\rm band} = \frac{\int F_\nu \left(\frac{\nu_0}{\nu}\right) R(\nu)\,{\rm d}\nu}{\int \left(\frac{\nu_0}{\nu}\right)^3 R(\nu)\,{\rm d}\nu}. \tag{8}$$

where $R(\nu)$ is the filter transmission (Fig. 1).

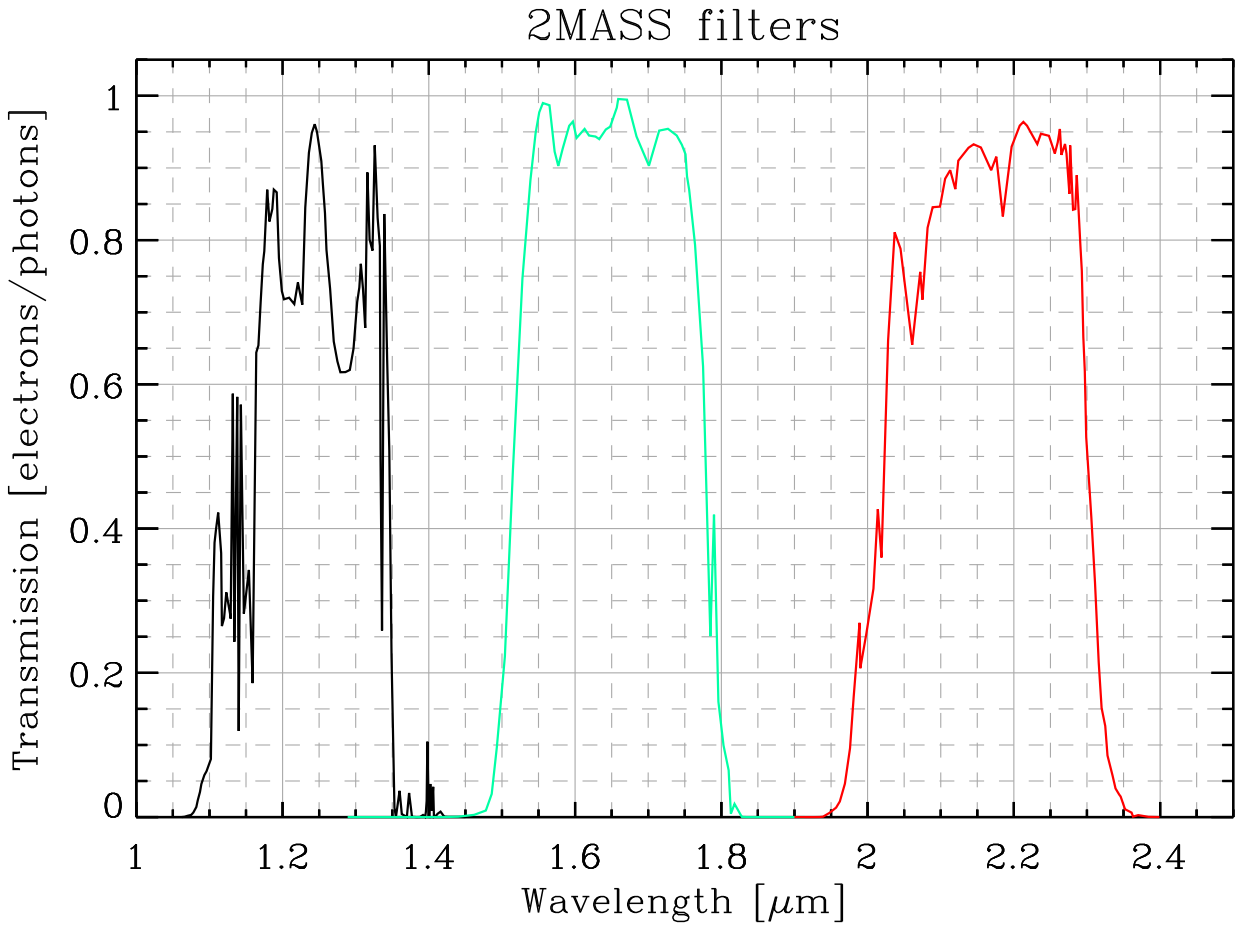

Figure 1: *2MASS filter transmission*. Dowloaded from here. This is the quantum efficiency (QE).

I could not find a table of color corrections. Thus I could not check the accuracy of my routine, except by comparing it to S. Hony's code (agreement better than 3 %).

2.2 Calibration errors

The calibration is not clear. Jarrett et al. (2003) quotes a $2-3\,\%$ uncertainty on the zero-point magnitude. Since it is not clear, we assume a non-correlated 3 % calibration error, to be conservative.

3 Akari FIS

3.1 Filters and Color Correction

According to the FIS DUM (version 1.3), the color correction convention assumes a $\nu F_\nu = const$ spectrum:

$$F_{\nu_0}^{\rm band} = \frac{\int \left(\frac{\nu_0}{\nu}\right) F_\nu R\,{\rm d}\nu}{\int \left(\frac{\nu_0}{\nu}\right)^2 R\,{\rm d}\nu}, \tag{9}$$

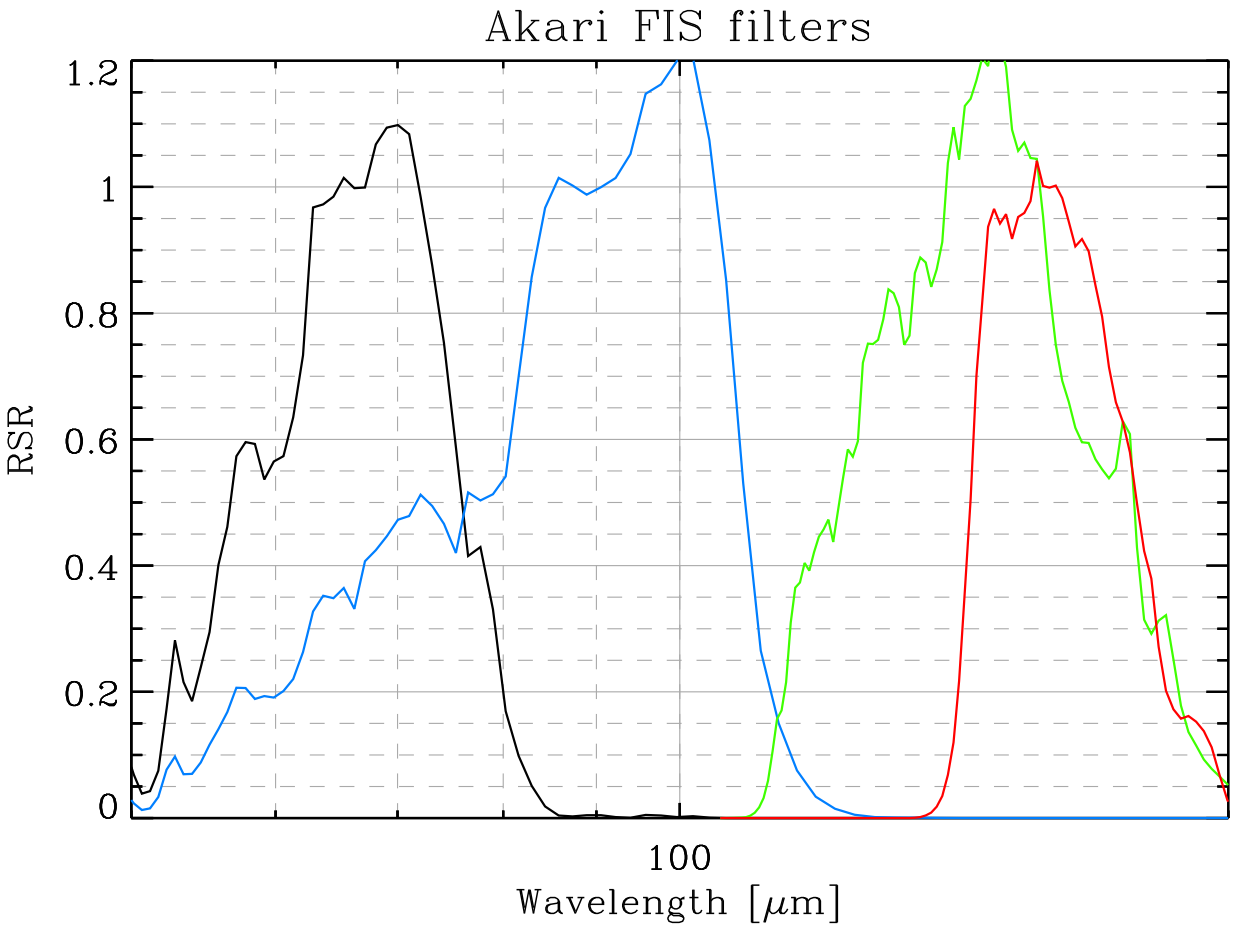

Figure 2: *FIS filter transmission.* Dowloaded from here. This is the relative spectral response (the quantum efficiency divided by ν and scaled).

where $R(\nu)$ is the filter transmission (Fig. 2).

We have compared our routine to the color correction given in Table 4.2.2 of FIS DUM (version 1.3), and the agreements are better than $0.4\,\%$.

3.2 Calibration errors

According to the FIS DUM (version 1.3), the calibration error is "*crudely*" estimated to be $\simeq 20\,\%$ in the SW band and $\simeq 30\,\%$ inn the LW band. No correlation is specified.

4 Akari IRC

4.1 Filters and Color Correction

According Sect. 4.8 of the Akari Data User Manual (version 1.3), the flux quoted by the pipeline, $F_\nu^{\rm band}$, is related to the actual flux F_ν (the SED) and the transmission $R(\nu)$ (in electrons/photons; Fig. 3) by:

$$F_{\nu_0}^{\rm band} = \frac{\int \left(\frac{\nu_0}{\nu}\right) F_\nu R \,{\rm d}\nu}{\int \left(\frac{\nu_0}{\nu}\right)^2 R \,{\rm d}\nu}, \tag{10}$$

where ν_0 is the nominal frequency. We have tested this equation, using the filters downloaded from here. These

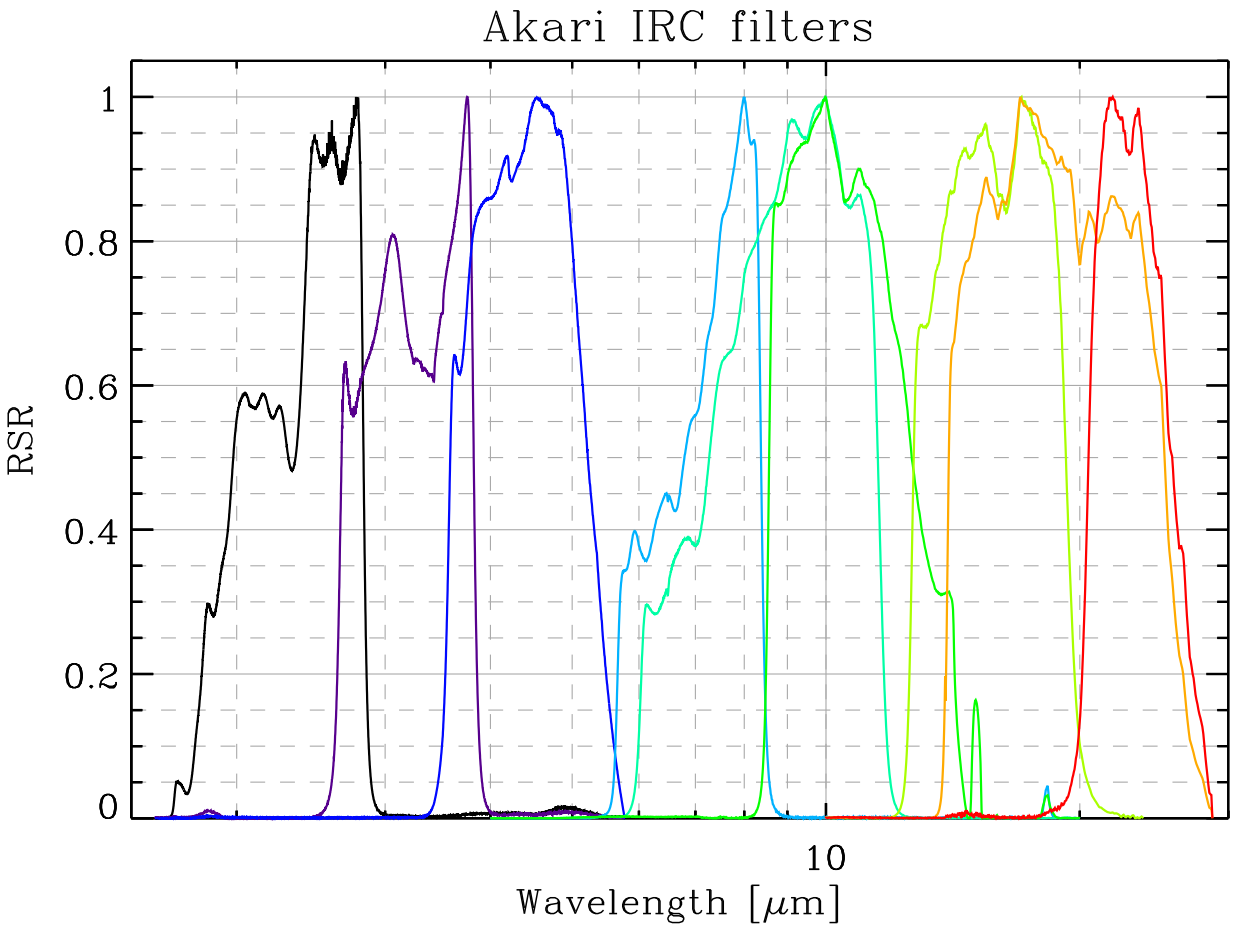

Figure 3: *Akari IRC transmission*. Downloaded from here. This is the relative spectral response (the quantum efficiency divided by ν and scaled).

filters are actually $R_\nu(\nu) = R(\nu)/\nu$. Our routine is in agreement with Tables 4.8.8 and 4.8.11 of the Akari Data User Manual (version 1.3), with an accuracy better than $1\,\%$.

4.2 Calibration errors

Table 4.6.7 of the Akari Data User Manual (version 1.3) quotes calibration uncertainties of each band, for point sources, ranging between 2 and 6 %. The degree of correlation between these calibration uncertainties is not clear from reading the manual. The calibration unceratinty of extended sources is not quantified either.

5 IRAS

5.1 Filters and Color Correction

According to the IRAS documentation, the color correction convention assumes a $\nu F_\nu = const$ spectrum:

$$F_{\nu_0}^{\text{band}} = \frac{\int \left(\frac{\nu_0}{\nu}\right) F_\nu R \, \mathrm{d}\nu}{\int \left(\frac{\nu_0}{\nu}\right)^2 R \, \mathrm{d}\nu}, \tag{11}$$

where $R(\nu)$ is the filter transmission (Fig. 4).

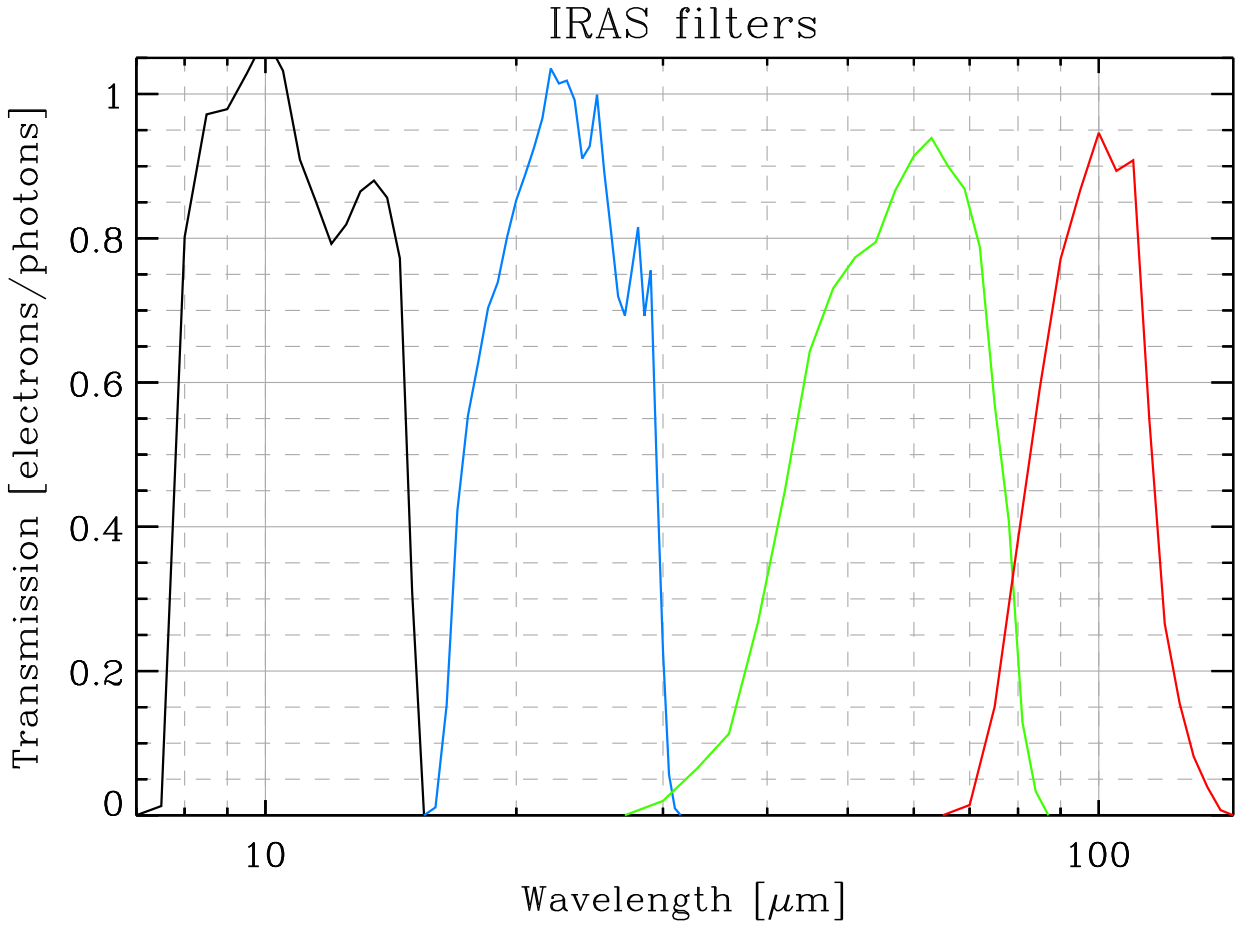

Figure 4: *IRAS filter transmission*. Dowloaded from here. This is the quantum efficiency (QE).

We have compared our routine to both power-laws and black bodies, given by the IRAS online documentation. It is accurate better than 1 %, except for a power-law with $\alpha = 3$.

5.2 Calibration errors

According to the IRAS explanatory supplement, the point source calibration of $\text{IRAS}_{12\mu m}$ is performed on α-Tau, the $\text{IRAS}_{25\mu m}$ and $\text{IRAS}_{60\mu m}$ extrapolation is made via models of stars. $\text{IRAS}_{60\mu m}$ and $\text{IRAS}_{100\mu m}$ are calibrated with asteroids. The uncertainties at 12, 25, and 60 μm, relative to the ground based 12 μm are 2, 5 and 5 %. The absolute uncertainty on the 12 μm is 4 %, common to the three bands. The correlation coefficients are therefore: $\rho_{\text{IRAS1,IRAS2}} = 0.56$, $\rho_{\text{IRAS1,IRAS3}} = 0.56$ and $\rho_{\text{IRAS2,IRAS3}} = 0.39$. The uncertainty at 100 μm is 10 %.

The extended source calibration was based on the point source calibration. I could not find a document quantifying the additional errors due to the the fact that the source is extended.

6 Herschel PACS

6.1 Filters and Color Correction

The ICC report (May 2013) relates the PACS band flux to the SED (F_ν) by:

$$F_{\nu_0}^{\text{band}} = \frac{\int F_\nu R \, \mathrm{d}\nu}{\int \left(\frac{\nu_0}{\nu}\right) R \, \mathrm{d}\nu}, \tag{12}$$

where $R(\nu)$ is the filter transmission times the bolometer absorption.

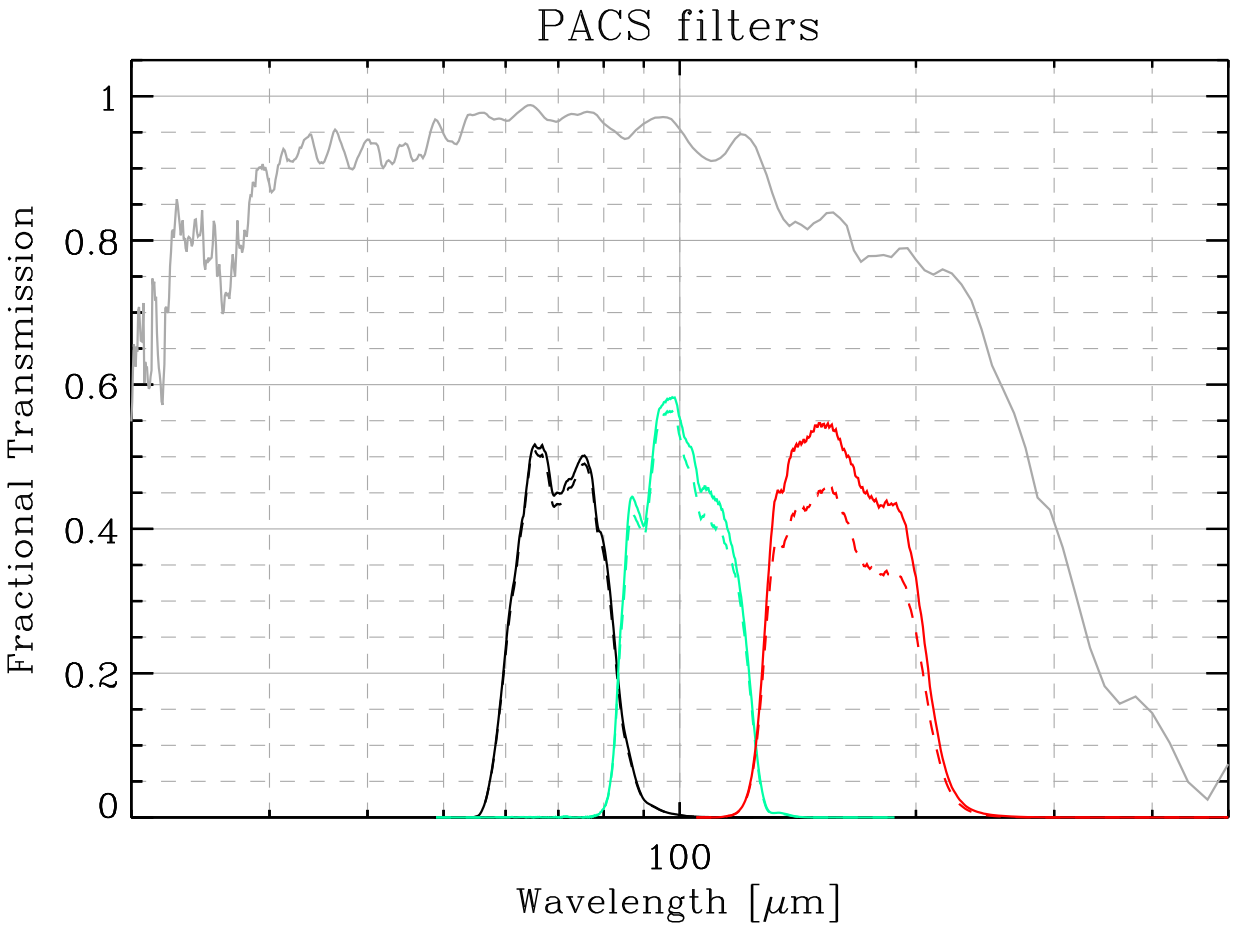

Figure 5: *PACS filter transmission* and bolometer absorption (in grey). Downloaded from here. This is not the quantum efficiency (QE). To obtain the QE, one would have to divide these profiles by λ.

We have tested this equation, using the filters downloaded from here (Fig. 5). We have compared it to Tables 2 (black bodies) of the ICC report (May 2013), and the results are in agreement to better than 1 %.

6.2 Calibration errors

The calibration of PACS is performed on 5 fiducial stars (Müller *et al.* 2011; Sect. 6). The model uncertainty is about 5 % and the RMS of the calibrator observations are 1.4 %, 1.6 % and 3.5 % in $\text{PACS}_{70\mu m}$, $\text{PACS}_{100\mu m}$ and $\text{PACS}_{160\mu m}$, respectively. The calibration errors, for point sources are therefore $\sigma_c = \sqrt{rms^2 + 0.05^2/5}$, which is 2.6 %, 2.8 % and 4.2 %. There is correlation between the modelled fluxes. The correlation coefficients are $\rho_{\text{IRAC1,IRAC2}} = 0.69$, $\rho_{\text{IRAC1,IRAC3}} = 0.45$ and $\rho_{\text{IRAC2,IRAC3}} = 0.44$.

The calibration for extended sources, is likely higher than those. However, we could not find publications qunatifying it exactly.

7 Herschel SPIRE

7.1 Filters and Color Correction

According to SPIRE observer's manual (version 2.4), the quoted flux in band for a point source is (same convention as PACS): relates the PACS band flux to the SED (F_ν) by:

$$F_{\nu_0}^{\rm band} = \frac{\int F_\nu R \, {\rm d}\nu}{\int \left(\frac{\nu_0}{\nu}\right) R \, {\rm d}\nu}, \tag{13}$$

where $R(\nu)$ is the filter transmission, and for extended sources, the transmission is weighted by λ^2:

$$F_{\nu_0}^{\rm band} = \frac{\int \left(\frac{\nu_0}{\nu}\right)^2 F_\nu R \, {\rm d}\nu}{\int \left(\frac{\nu_0}{\nu}\right)^3 R \, {\rm d}\nu}. \tag{14}$$

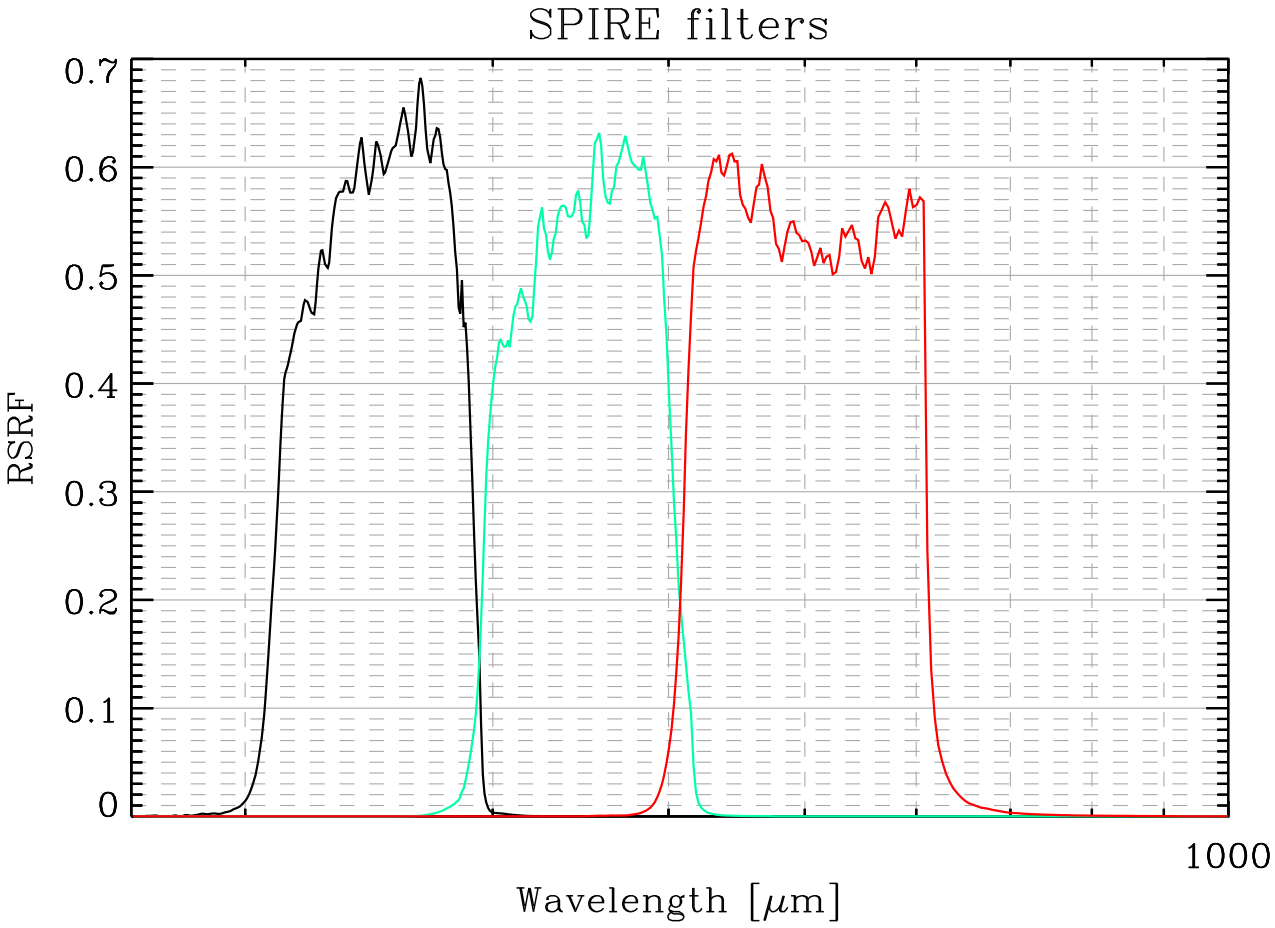

Figure 6: *Point source SPIRE RSRFs*. Downloaded from here.

We have tested our routine on power-law spectra and compared to Table 5.3 of the SPIRE observer's manual (version 2.4), for both point and extended sources, using the filters of Fig. 6. They are accurate better than $0.2\,\%$.

7.2 Calibration errors

According to SPIRE observer's manual (version 2.4; Sect. 5.2.8), if the data are *point source calibrated* only, the fluxes of extended sources must be multiplied by (0.9828,0.9834,0.9710).

The calibration errors, detailed by Griffin et al. (2013), are summarized on SPIRE calibration page:

- $4\,\%$ due to the uncertainty on the Neptune model (correlated across the three bands);
- $1.5\,\%$ due to the noise of the observations of Neptune (independent);
- $4\,\%$ due to the beam area, for extended sources, only (independent).

Thus the calibration errors are $5.9\,\%$, for each band, with the correlation coefficient $\rho = 0.47$.

8 MSX Galactic Plane Survey

8.1 Filters and Color Correction

According to Egan et al. (1999, App. D), the quoted flux is related to the SED by:

$$F_{\nu_0}^{\text{band}} = \frac{\int F_\nu R(\nu)\,\mathrm{d}\nu}{\Delta\nu_0}, \tag{15}$$

where $R(\nu)$ is the relative spectral response of Fig. 7, and the isophotal bandwidths are:

$$\Delta\lambda_0(A) = 3.36\ \mu m \tag{16}$$
$$\Delta\lambda_0(C) = 1.72\ \mu m \tag{17}$$
$$\Delta\lambda_0(D) = 2.23\ \mu m \tag{18}$$
$$\Delta\lambda_0(E) = 6.24\ \mu m. \tag{19}$$

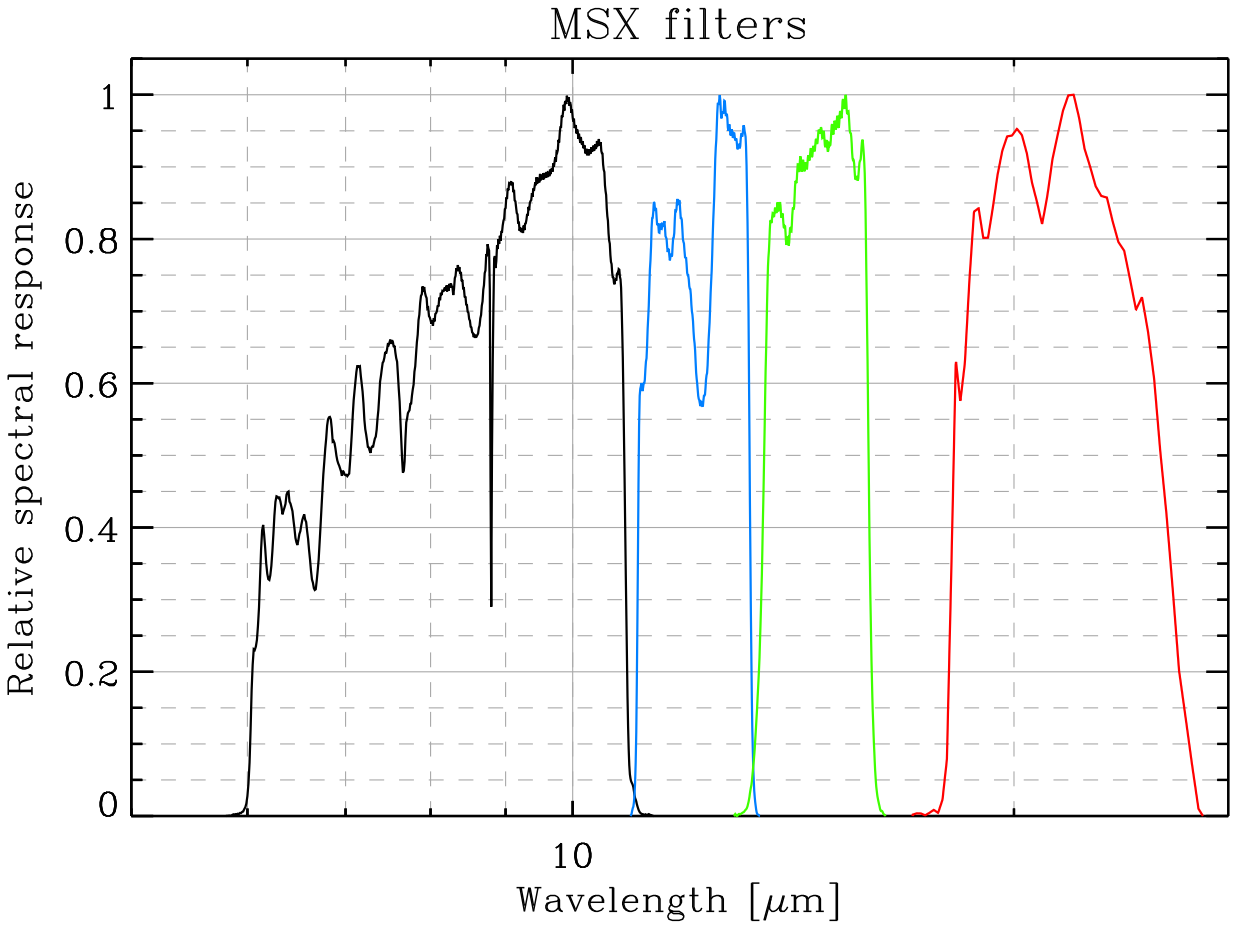

Figure 7: *MSX filter transmission A, C, D & E.* Dowloaded from here.

We have tested our routine on power-law spectra and compared to Table D-4 of Egan et al. (1999), using the filters of Fig. 7. They are accurate better than $0.6\,\%$.

8.2 Calibration errors

According to Egan et al. (1999), the calibration was performed both on the ground and in flight, on standard objects. It appears that the calibration uncertainty is dominated by the noise of the calibrator observations, making the correlation between bands negligible. For the Galactic plane survey, the extended source calibration uncertainties are $9\,\%$, $8\,\%$, $9\,\%$ & $15\,\%$, for A, C, D & E, respectively.

9 Planck HFI

9.1 Filters and Color Correction

According to Planck Collaboration et al. (2014, Eq. 2), the quoted flux is related to the SED by:

$$F_{\nu_0}^{\text{band}} = \frac{\int F_\nu R(\nu)\,\mathrm{d}\nu}{\int \left(\frac{\nu_0}{\nu}\right) R(\nu)\,\mathrm{d}\nu}. \tag{20}$$

This is the synthetic photometry for a bolometer array, with the $\nu F_\nu = const$ convention.

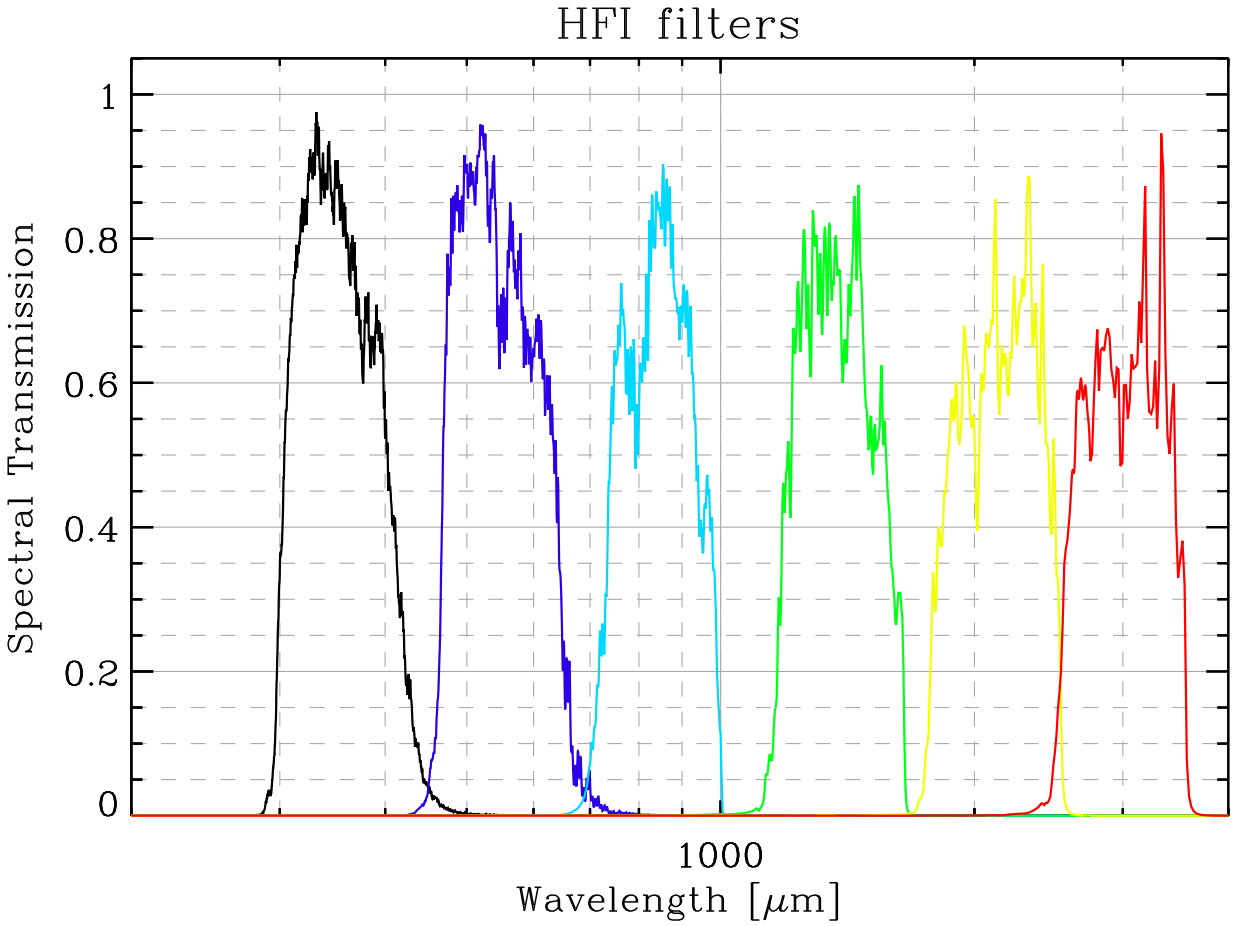

Figure 8: *HFI filter transmission*. Dowloaded from here. This is not the quantum efficiency (QE), since HFI is a bolometer array.

We have compared our colour correction routine to the values given by the UC CC software notes, for both power-laws and black bodies. The results are in agreement with an accuracy better than $1\,\%$, except for the two short wavelength bands for a power-laws with indices $\alpha = -3, -4$, where the interpolation is steep.

9.2 Calibration errors

According to Planck Collaboration et al. (2014), the calibration of HFI is performed using Neptune and Uranus for the 545 and 857 GHz bands, and using the CMB dipole for the low frequencies. The various sources of uncertainties are summarized in Table 11 of Planck Collaboration et al. (2014). The last column ("*model*") is the only one that induces a correlation between wavelengths.

10 Spitzer IRAC

10.1 Filters and Color Correction

According to the IRAC Instrument Handbook (version 2.0.3; Eq. 4.8), the flux quoted by the pipeline, $F_\nu^{\rm band}$, is related to the actual flux F_ν (the SED) and the transmission $R(\nu)$ (in electrons/photons; Fig. 9) by:

$$F_{\nu_0}^{\rm band} = \frac{\int \left(\frac{\nu_0}{\nu}\right) F_\nu R \, {\rm d}\nu}{\int \left(\frac{\nu_0}{\nu}\right)^2 R \, {\rm d}\nu}, \tag{21}$$

where ν_0 is the nominal frequency. We have tested this equation, using the filters downloaded from here.

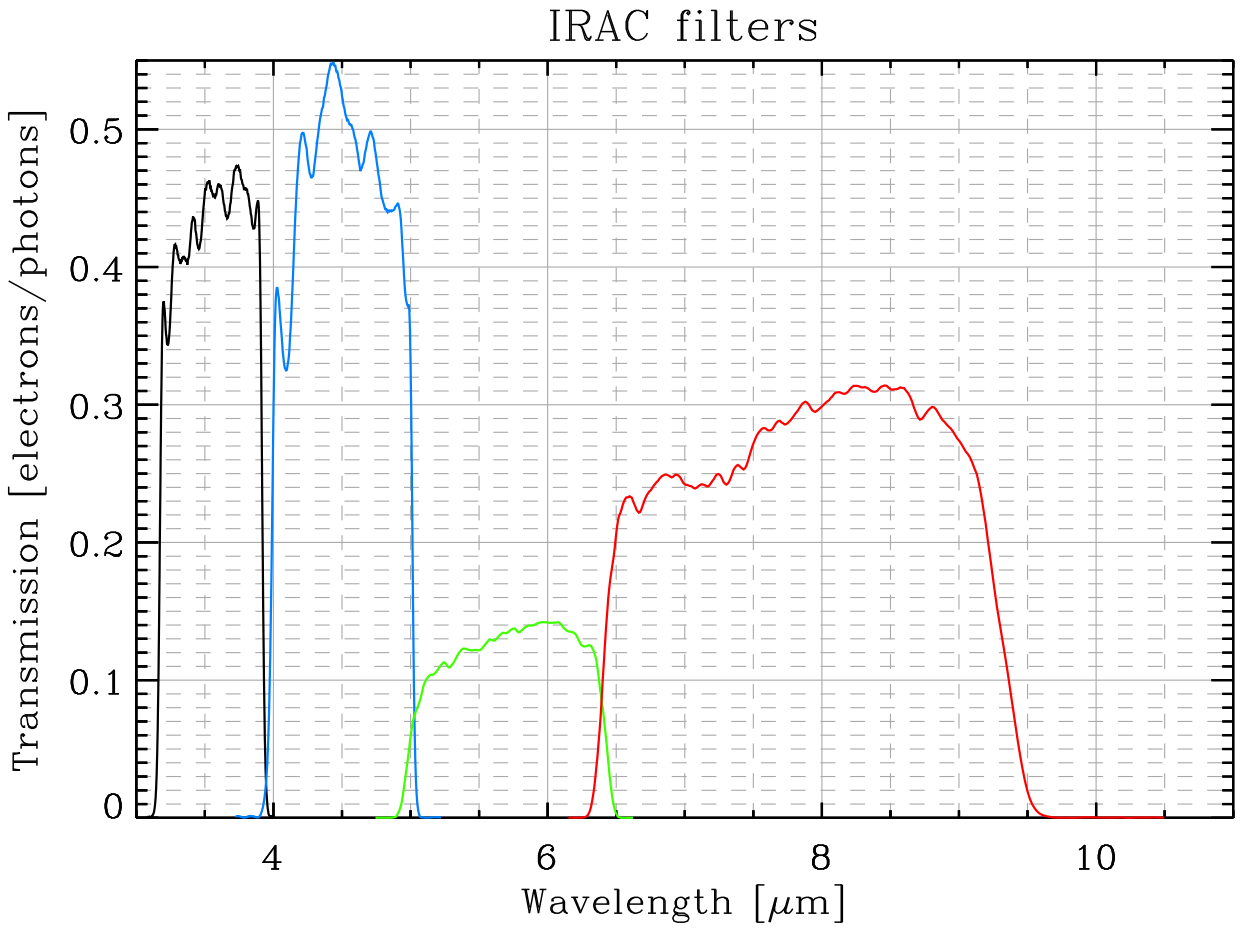

Figure 9: *IRAC transmission*. Downloaded from here. This is the quantum efficiency (QE).

We have compared it to Tables 4.3 (power-law) and 4.4 (black body) of the IRAC Instrument Handbook (version 2.0.3), and the results are in agreement to better than $0.2\,\%$.

10.2 Calibration errors

For extended sources, with a relatively flat surface brightness profile, the IRAC Instrument Handbook (version 2.0.3; Sect. 4.11.2) advises to apply aperture correction factors, for the infinite case of 0.91, 0.94, 0.73, 0.74 for IRAC$_{3.6\mu m}$, IRAC$_{4.5\mu m}$, IRAC$_{5.8\mu m}$, and IRAC$_{8\mu m}$ respectively. These apertures are accurate to $10\,\%$ (independent between wavelengths). This error should probably not be accounted as "*systematic error*", as it depends on the actual morphology of the source, and therefore it is going to vary from one to place to another on a given image. Indeed, these aperture correction factors were derived from the surface brightness profile of elliptical galaxies.

Reach et al. (2005) quote a $2\,\%$ calibration error in all IRAC bands. According to Eq. (13) of Reach et al. (2005), it appears that $\sigma_{\rm abs}$ is the only correlated term error. Thus, the interband correlation coefficient is $\rho \simeq 0.29$.

11 Spitzer MIPS

11.1 Filters and Color Correction

According to the MIPS Instrument Handbook (version 3; Eq. 4.2), the flux quoted by the pipeline, $F_\nu^{\rm band}$, is related to the actual flux F_ν (the SED) and the transmission $R(\nu)$ (in electrons/photons; Fig. 10) by:

$$F_{\nu_0}^{\rm band} = \frac{\int F_\nu R \,{\rm d}\nu}{\int \frac{B_\nu(\nu,T_0)}{B_\nu(\nu_0,T_0)} R \,{\rm d}\nu} \simeq \frac{\int F_\nu R \,{\rm d}\nu}{\int \left(\frac{\nu}{\nu_0}\right)^2 R \,{\rm d}\nu}, \tag{22}$$

with $T_0 = 10^4$ K. Note here that there is a λ factor missing in each integral compared to the Handbook. This is because the handbook requires to integrate over $R_\lambda(\lambda) = \lambda R(\lambda)$.

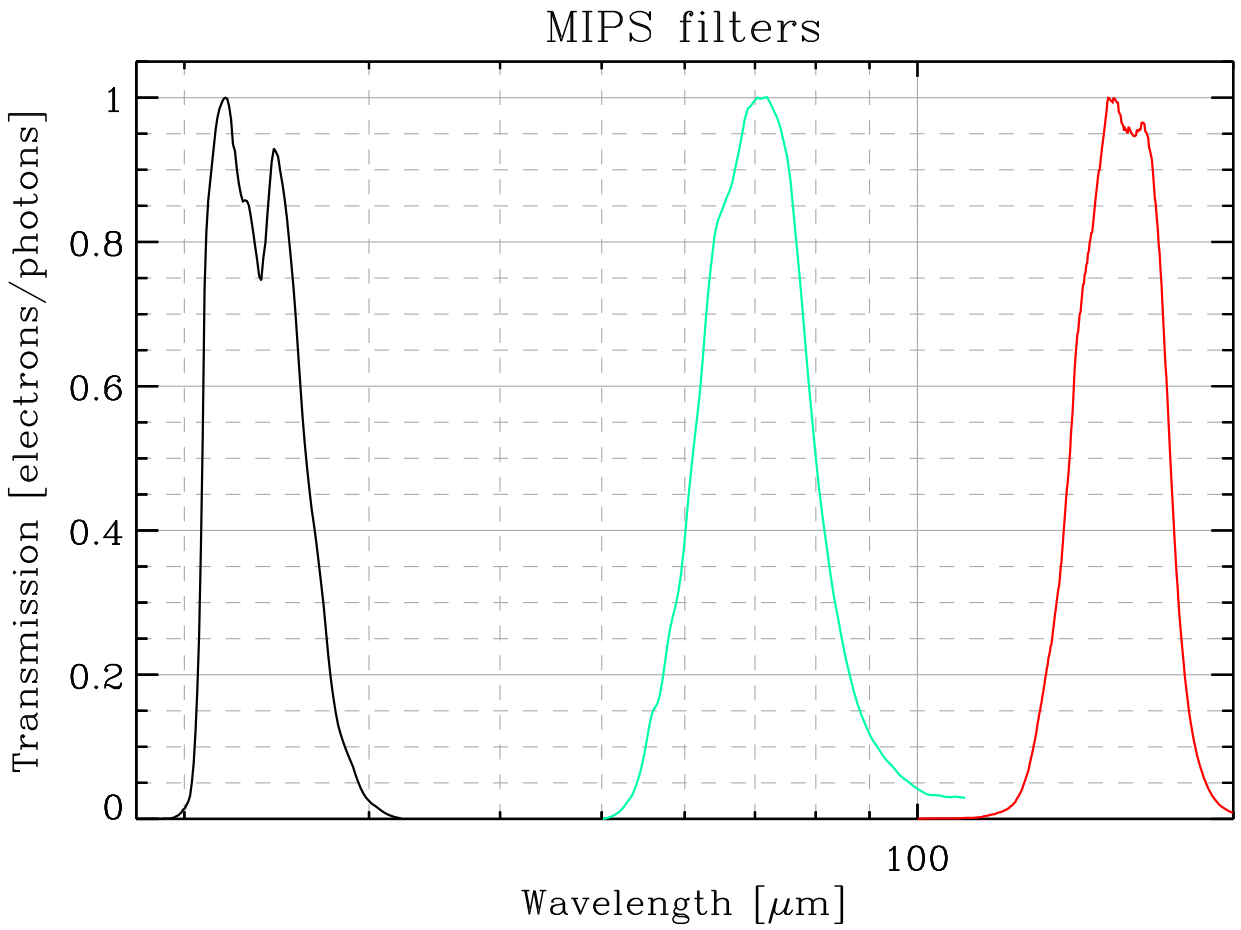

Figure 10: *MIPS transmission.* Downloaded from here. This is the quantum efficiency (QE).

We have tested this equation, using the filters downloaded from here. We have compared it to Tables 4.17 (power-law) and 4.16 (black body) of the MIPS Instrument Handbook (version 3), and the results are in agreement to better than 1 %, for the whole range of parameters.

11.2 Calibration errors

The MIPS Instrument Handbook (version 3; Sect. 4.1.3) quotes a point source calibration error of 4 % for MIPS$_{24\mu m}$ (Engelbracht et al., 2007), 5 % for MIPS$_{70\mu m}$ (Gordon et al., 2007) and 12 % for MIPS$_{160\mu m}$ (Stansberry et al., 2007). It also states that the calibration of extended sources is consistent with these values.

The samples used for calibration are different for each instrument. The primary calibrators are A stars for MIPS$_{24\mu m}$, B and M stars for MIPS$_{70\mu m}$ and asteroids for MIPS$_{160\mu m}$. However, the calibration of MIPS$_{160\mu m}$ is made using the MIPS$_{24\mu m}$ and MIPS$_{70\mu m}$ observations of asteroids. Therefore, we can consider that the calibration uncertainties of MIPS$_{24\mu m}$ and MIPS$_{70\mu m}$ are independent, but that they are correlated with MIPS$_{160\mu m}$. The correlation coefficients are: $\rho_{\rm MIPS1,MIPS3} \simeq 0.33$, $\rho_{\rm MIPS2,MIPS3} \simeq 0.42$.

12 WISE

12.1 Filters and Color Correction

According to the online documentation, using the filters of Fig. 11, the color correction is:

$$F_{\nu_0}^{\text{band}} = \frac{\int \left(\frac{\nu_0}{\nu}\right) F_\nu R \, \mathrm{d}\nu}{\int \left(\frac{\nu_0}{\nu}\right)^3 R \, \mathrm{d}\nu}. \tag{23}$$

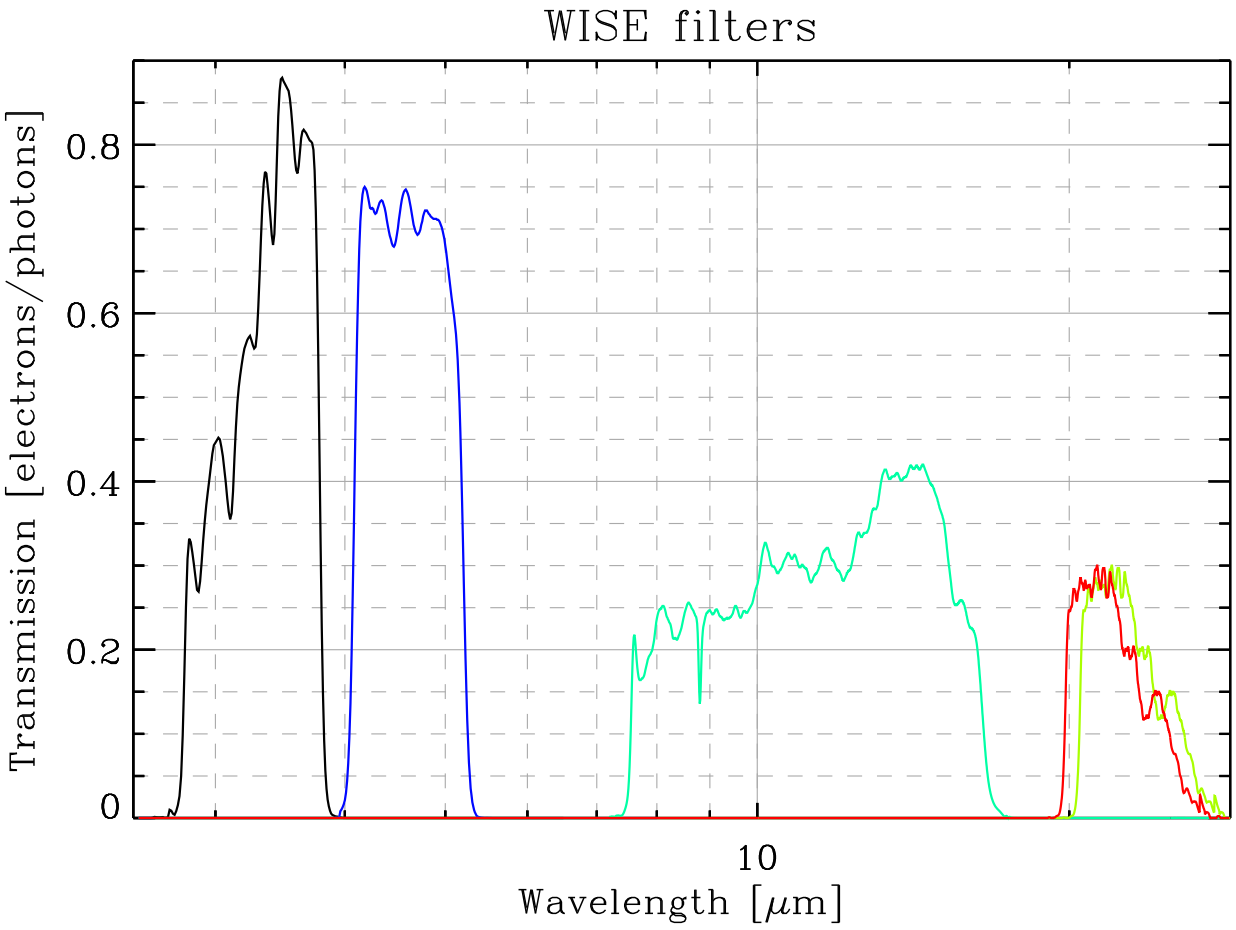

Figure 11: *WISE filter transmission*. Dowloaded from here. This is not the quantum efficiency (QE). To obtain the QE, one would have to divide these profiles by λ.

We have compared our routine to the results of Wright et al. (2010, or here), for power-law and black bodies. The results are in agreement, better than $0.2\,\%$.

We also implement the revision of WISE4 by Brown et al. (2014), which simply consists in increasing the wavelength of the original RSRF by $3.3\,\%$.

12.2 Calibration errors

The calibration of WISE is a mess. It is performed on observations of stars toward the Galactic pole, and tied to IRAC, MIPS, IRS and MSX by Jarrett et al. (2011). The rms part of the calibration error (independent between wavelengths; proper to WISE) is 2.4, 2.8, 4.5 and $5.7\,\%$. To simplify, we can add and correlate the WISE1 and IRAC1 calibration errors, the WISE2 and IRAC2, the WISE3 and IRS-SL/LL and WISE4 and MIPS1. According to Decin et al. (2004), the IRS-LL calibration uncertainty is $\simeq 15\,\%$. In summary:

WISE1: $\sigma_{\text{cal}} = 3.2\,\%$ and $\rho_{\text{WISE1,IRAC1}} = 0.66$;

WISE2: $\sigma_{\text{cal}} = 3.5\,\%$ and $\rho_{\text{WISE2,IRAC2}} = 0.59$;

WISE3: $\sigma_{\text{cal}} = 15.7\,\%$ and $\rho_{\text{WISE3,IRS-LL}} = 0.96$.

WISE4: $\sigma_{\text{cal}} = 13.3\,\%$ and $\rho_{\text{WISE4,MIPS1}} = 0.30$.

13 DIRBE

13.1 Filters and Color Correction

According to the DIRBE explanatory supplement, using the filters of Fig. 12, the color correction is:

$$F_{\nu_0}^{\text{band}} = \frac{\int F_\nu R \, \mathrm{d}\nu}{\int \left(\frac{\nu_0}{\nu}\right) R \, \mathrm{d}\nu}. \tag{24}$$

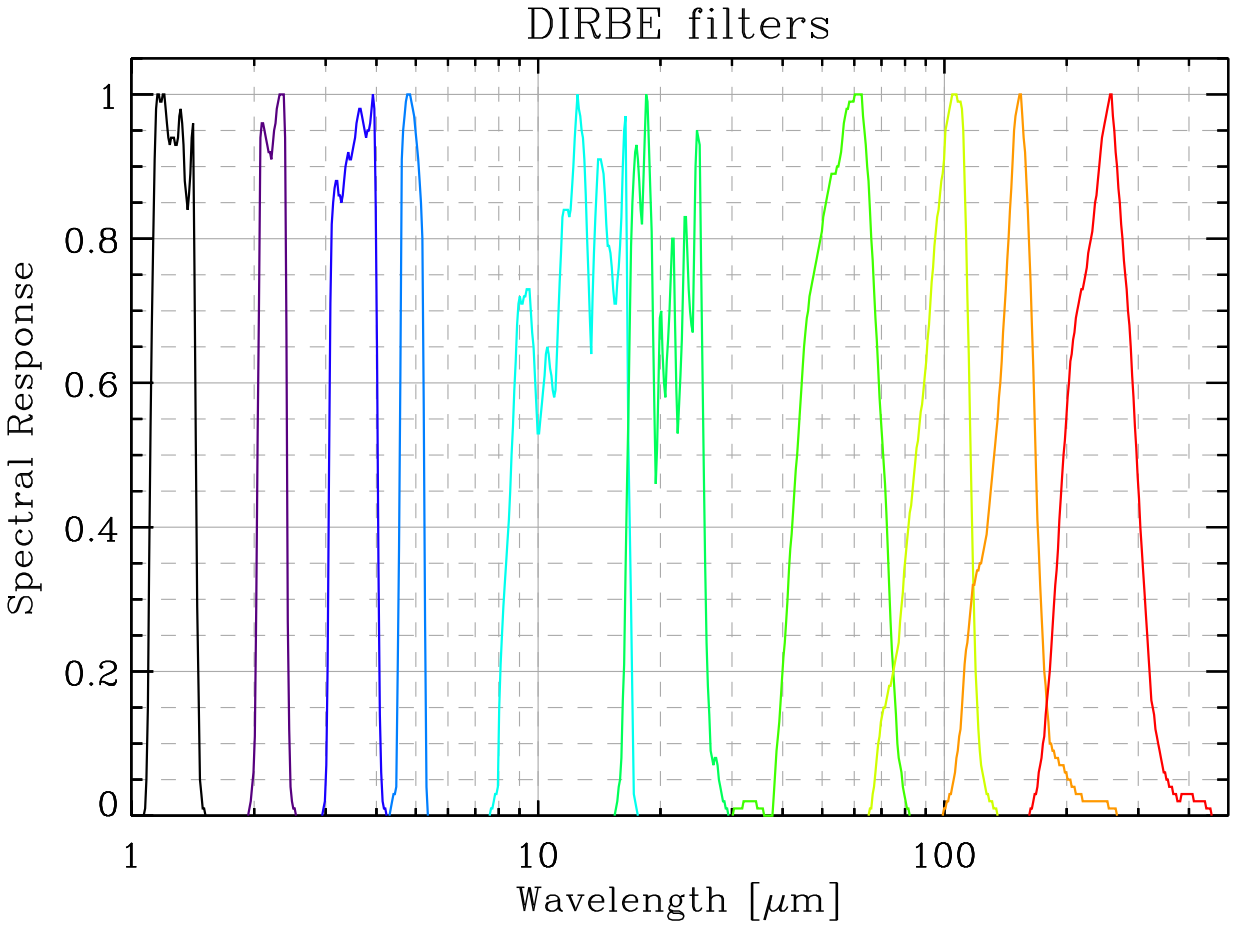

Figure 12: *DIRBE spectral response.* Dowloaded from here. This is not the quantum efficiency (QE).

We have compared our routine to the results of the Appendix B of the DIRBE explanatory supplement, for power-laws. The results are in agreement, better than $0.6\,\%$.

13.2 Calibration errors

The documentation on DIRBE calibration is very scarce. The first Table of Burdick & Murdock (1997) gives the absolute calibration uncertainties of each band, as well as the name of their calibrator, for the Mark 3 calibration (July 1995).

- Bands 1 to 5 were calibrated on Sirius, with a $3\,\%$ uncertainty for bands 1 to 4 et $4\,\%$ for band 5.
- Band 6 was calibrated on NGC 7027 with a calibration uncertainty of $15\,\%$.
- Bands 7 and 8 were calibrated on Uranus, with calibration uncertainties of $11\,\%$ and $13\,\%$, respectively.
- Bands 9 and 10 were calibrated on Jupiter, with calibration uncertainties of $11\,\%$ and $12\,\%$, respectively.

The correlation between these calibration uncertainties is not discussed. However, Fixsen et al. (1997) quote a relative stability of the gain of $\simeq 1\,\%$ over the course of the mission. The best we can do is the following. We assume that bands calibrated on different calibrators are independent. We assume that bands calibrated on the same calibrator are only partially correlated, due to the $\simeq 1\,\%$ drift.

14 NIKA2

14.1 Filters and Color Correction

According to Eqs. (17) and (18) of Perotto et al. (2020), the NIKA2 fluxes are:

$$F_\nu^{\rm band}(\nu_0) = \frac{\int F_\nu(\nu) T(\nu)\,{\rm d}\nu}{\int \left(\frac{\nu}{\nu_0}\right)^{1.6} T(\nu)\,{\rm d}\nu}. \tag{25}$$

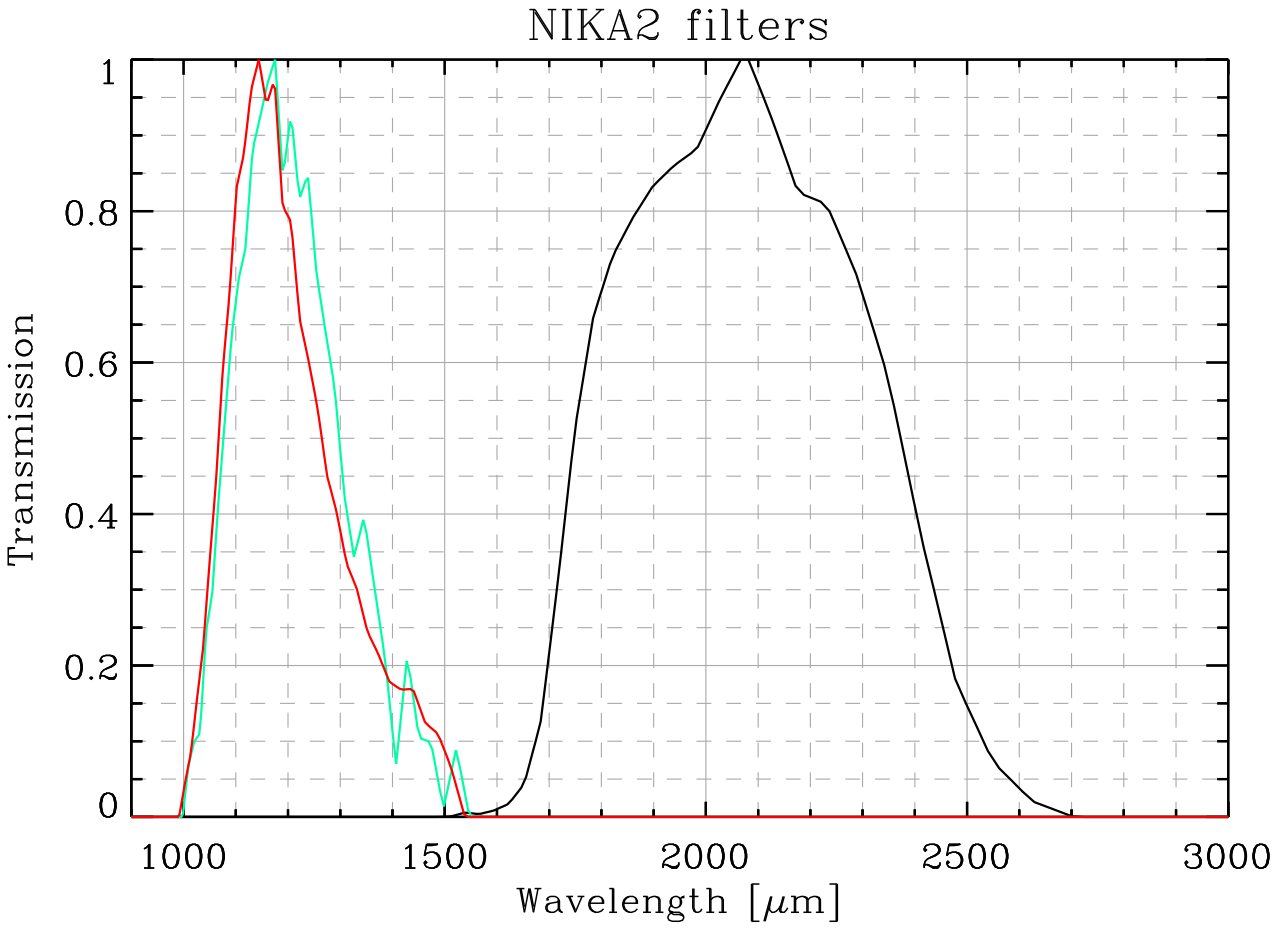

Figure 13: *NIKA2 spectral response.* There are two filters at 1mm, as they correspond to the two polarization directions.

We have compared our routine, using the filters of Fig. 13, to Table 12 of Perotto et al. (2020). The results are in agreement, better than $0.4\,\%$.

14.2 Calibration errors

The calibration is presented by Perotto et al. (2020). The calibrators are Uranus and Neptune. The absolute calibration uncertainty at both wavelength is $5\,\%$ and appears to be dominated by the scatter in the observations of the calibrators, the skydip corections and the beam efficiency correction for extended sources. All these uncertainty sources are independent at both wavelengths. We thus assume that these uncertainties are uncorrelated.

References

Brown, M. J. I., Jarrett, T. H., & Cluver, M. E. 2014, Publications of the Astronomical Society of Australia, 31, e049

Burdick, S. V. & Murdock, T. L. 1997, COBE Final Report: DIRBE Celestial Calibration, Tech. rep., NASA

Decin, L., Morris, P. W., Appleton, P. N., et al. 2004, ApJS, 154, 408

Egan, M. P., Price, S. D., Moshir, M. M., Cohen, M., & Tedesco, E. 1999, NASA STI/Recon Technical Report N, 14854

Engelbracht, C. W., Blaylock, M., Su, K. Y. L., et al. 2007, PASP, 119, 994

Fixsen, D. J., Weiland, J. L., Brodd, S., et al. 1997, ApJ, 490, 482

Gordon, K. D., Engelbracht, C. W., Fadda, D., et al. 2007, PASP, 119, 1019

Griffin, M. J., North, C. E., Schulz, B., et al. 2013, MNRAS, 434, 992

Jarrett, T. H., Chester, T., Cutri, R., Schneider, S. E., & Huchra, J. P. 2003, AJ, 125, 525

Jarrett, T. H., Cohen, M., Masci, F., et al. 2011, ApJ, 735, 112

Perotto, L., Ponthieu, N., Macías-Pérez, J. F., et al. 2020, A&A, 637, A71

Planck Collaboration, Ade, P. A. R., Aghanim, N., et al. 2014, A&A, 571, A8

Reach, W. T., Megeath, S. T., Cohen, M., et al. 2005, PASP, 117, 978

Stansberry, J. A., Gordon, K. D., Bhattacharya, B., et al. 2007, PASP, 119, 1038

Wright, E. L., Eisenhardt, P. R. M., Mainzer, A. K., et al. 2010, AJ, 140, 1868